Radar Signatures of a Passenger Car

Gintautas Palubinskas and Hartmut Runge

***Abstract*—Upcoming new synthetic aperture radar (SAR) satellites such as TerraSAR-X and Radarsat-2 offer high spatial image resolution and dual receive antenna capabilities, which open new opportunities for worldwide traffic monitoring applications. If the radar cross section (RCS) of the vehicles is strong enough, they can be detected in the SAR data, and their speed can be measured. For system performance prediction and algorithm development, it is therefore indispensable to know the RCS of typical passenger cars. The geometry parameters that have to be considered are the radar look direction, incidence angle, and vehicle orientation. In this letter, the radar signatures of nonmoving or parking cars are presented. They are measured experimentally from airborne experimental SAR (E-SAR) data, which have been collected during flight campaigns in 2005 and 2006 with multiple overflights at different aircraft headings. The radar signatures could be measured for the whole range of aspect angles from 0° to 180° and with high angular resolution due to the large synthetic aperture length of the E-SAR radar sensor. The analysis for one type of passenger car and particular incidence angles showed that the largest radar cross-sectional values and, thus, the greatest chance of detection of the vehicles appear when the car is seen from the front, back, and side. Radar cross-sectional values for slanted views are much lower and are therefore less suitable for car detection. The measurements have been performed in the X-band (9.6 GHz) with VV-polarization, and at incidence angles of 41.5° and 42.5°. The derived radar signature profile can also be used for the verification of radar cross-sectional simulation studies.**

***Index Terms*—Airborne experimental synthetic aperture radar (E-SAR) sensor, aspect angle, look processing, radar cross section (RCS), road vehicles, traffic monitoring.**

I. Introduction

THE GERMAN radar satellite TerraSAR-X carries a high-resolution dual-receive-antenna (DRA) synthetic aperture radar (SAR) sensor and is scheduled for launch in 2007 [1], [2]. Due to the DRA mode, it will have the capability to acquire the along-track interferometry data that will allow it to measure the velocity of moving targets and thus can be useful for traffic monitoring applications on a global scale.

The German Aerospace Center (DLR) is already developing a processing system called "traffic processor," which will detect cars, measure their speed, and assign them to the road network [3]–[9]. For the implementation of the vehicle detection algorithms, based on the statistical theory, the knowledge of the radar signatures of a vehicle is of high importance, particularly, under consideration of the geometry of the radar look direction and the vehicle orientation. The radar cross section (RCS) for various military targets is well known, but for civilian road vehicles, this information is still missing or insufficient. Simulation of radar signatures is a very difficult task due to the lack of available realistic physical models of vehicles and backgrounds [10].

For the development and testing of the processing algorithms, two airborne SAR flight campaigns have been conducted with DLR experimental SAR sensor E-SAR. SAR data have been collected for one frequency (X-band) and one polarization (VV). In total, 11 test cars of exactly the same type but with different orientations have been placed in empty car parks in order to cover a whole range of aspect angles with only few overflights. The RCS analysis is performed for this type of car (the most popular car in Germany) dependent on the aspect angle.

This letter provides a short introduction to the RCS measurement method, the look processing technique, and the radar sensor used in the experiments. Furthermore, the results of the investigations and some examples of radar signatures of a passenger car are presented.

II. Objective

The aim is to measure the RCS of a car from a focused single-look complex (SLC) slant-range SAR image. In general, the RCS may depend on radar parameters (frequency f and polarization p), car parameters (type (car or truck), model, shape, and material), geometry parameters (incidence angle and car aspect angle), and background parameters (road type, condition, etc.). For the definition of angles, see Fig. 1. The incidence angle θ is the angle between the line of sight of the radar sensor and the normal to the Earth surface, and has smaller values in the near range of the swath and larger ones in the far range. The car aspect angle α is the angle between the line of sight of the radar sensor projected to the ground and the car driving direction. For the back, side, and front views of a car, $\alpha = 0°$, $\alpha = 90°$, and $\alpha = 180°$, respectively. Thus, the RCS of a car is a function of a number of parameters and can be written in the following way: $\sigma(f, p, \theta, \alpha, \text{car}, \text{road})$.

RCS for a point target is defined as in [11]–[13]

$$\sigma(m^2) = \frac{1}{K} \int_{-\infty}^{\infty} \int_{-\infty}^{\infty} I_\sigma(x, y) \cdot dx \cdot dy$$

$$\approx \frac{1}{K} \cdot \Delta x \cdot \Delta y \cdot \sum_{k,l} I_\sigma(k, l) \qquad (1)$$

where K is a scaling factor and was equal to 1.0×10^6 for the experimental data used; Δx and Δy are the pixel spacing

Manuscript received January 17, 2007; revised April 13, 2007.

The authors are with the Remote Sensing Technology Institute, German Aerospace Center (DLR) Oberpfaffenhofen, 82234 Wessling, Germany (e-mail: Gintautas.Palubinskas@dlr.de; Hartmut.Runge@dlr.de).

Color versions of one or more of the figures in this paper are available online at http://ieeexplore.ieee.org.

Digital Object Identifier 10.1109/LGRS.2007.903074

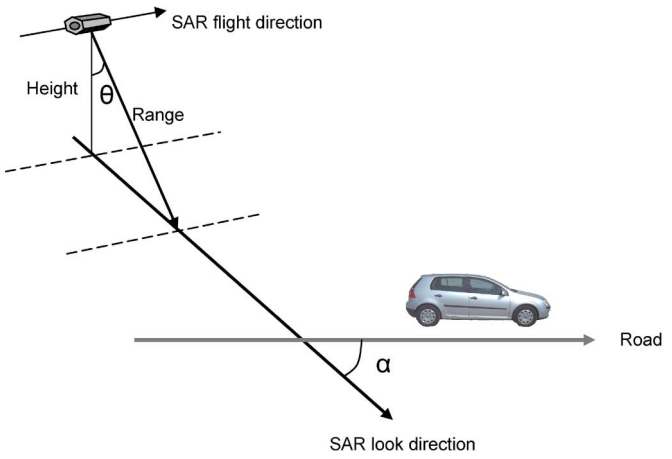

Fig. 1. Definition of incidence angle θ and aspect angle α. The incidence angle θ is the angle between the line of sight of the radar sensor and the normal to the Earth surface, and has smaller values in the near range of the swath and larger ones in the far range. The car aspect angle α is the angle between the line of sight of the radar sensor projected to the ground and the car driving direction. For the back, side, and front views of a car, $\alpha = 0°$, $\alpha = 90^{\alpha}$, and $\alpha = 180°$.

in azimuth and slant range, respectively; and $\sum_{k,l} l_\sigma(k,l)$ is the integrated power of a point target (radar brightness or beta values). We can rewrite the formula in decibels, i.e.,

$$\sigma(\mathrm{dB}\cdot\mathrm{m}^2) = -10\cdot\log K + 10\cdot\log(\Delta x\cdot\Delta y) + 10\cdot\log\sum_{k,l} I_\sigma(k,l) \quad (2)$$

where the first term is a calibration scale factor that is equal to -60 dB $\cdot$ m^2 in this case, and the last term is measured in SLC image with the DLR Image Analysis Software.

RCS can be estimated in two different ways: 1) simulated, if geometrical models of cars are available or 2) measured experimentally from SAR image data. In this letter, we consider the latter approach.

III. Data

The DLR airborne experimental radar sensor E-SAR was used during the flight campaigns for the acquisition of the radar image data. This system has been in use for different applications and has been continuously improved and extended over a period of more than 16 years. It is operated on a Do-228 aircraft. Detailed description of the sensor can be found in [14]. Table I lists the main E-SAR system, flight, and processing parameters used for the SAR experiments. Detailed description of the flight campaigns is given in the experimental part of this letter.

IV. Methodology

The large synthetic aperture length or beam width angle of approximately 7° of the airborne radar sensor E-SAR can be divided into several looks (subapertures), thus decreasing the target's illumination time or, equivalently, the spatial resolution in the azimuth direction. Due to a very high resolution in azimuth, e.g., several centimeters for X-band, it is even desirable to reduce this resolution in order to achieve approximately quadratic ground pixels.

TABLE I
E-SAR System and Experiment Parameters

Parameter	Value	Value
date of flight campaign	12.5.2005	8.5.2006
frequency band	X (9.6 GHz)	X (9.6 GHz)
polarization	VV	VV
range bandwidth	100 MHz	100 MHz
pulse repetition frequency	1000 Hz	1000 Hz
sensor forward velocity	88 m/s	90 m/s
altitude above MSL	4005 m	1833 m
incidence angle	20 – 60 deg	20 – 60 deg
resolution (rg x az)	2 m x 0.085 m	2 m x 0.1 m
SLC pixel spacing (rg x az)	1.5 m x 0.088 m	1.5 m x 0.09 m
number of looks	21	21
look bandwidth	52 Hz	52 Hz
look overlap	about 20 %	about 20 %
look beam width angle	0.35°	0.35°
car incidence angle θ	41.13° – 41.76°	42.03° – 43.05°
σ_0 of road in dB	-17	-25

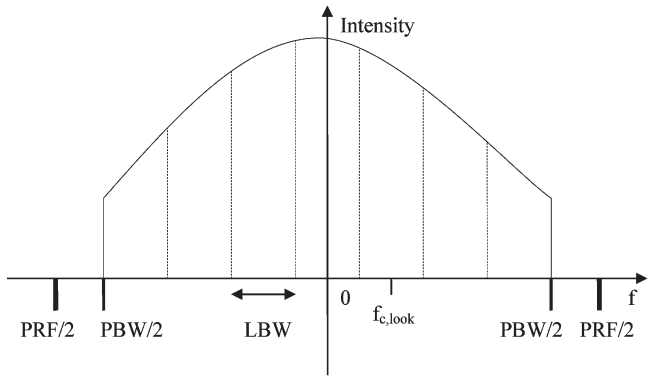

Fig. 2. Look processing in azimuth means that the processing bandwidth PBW is divided into several separately processed, maybe overlapping, looks with look bandwidth LBW and look center frequency $f_{c,\mathrm{look}}$. The look processing decreases the azimuth resolution and the target's illumination time, thus increasing the aspect angle resolution. For example, the processing of seven looks for a beam width angle of 7° will lead to the aspect angle resolution of 1°.

The looks represent different views of a target and allow us to increase the aspect angle resolution from 7° for full-azimuth-resolution SAR data to $7°/L$ for look-processed data, where L is the number of looks. The concept of this look processing, e.g., into seven looks, is illustrated in Fig. 2.

In the subsequent experiments, the following setup was used (see Table I). The whole processing bandwidth in azimuth was divided into 21 looks, and the look bandwidth of 52 Hz allowed us to receive approximately the beam width angle or aspect angle resolution of 0.35° and overlapping of looks about 20%.

V. Experiments

A. First Flight Campaign

The experimental data have been collected by DLR airborne E-SAR sensor during a flight campaign on May 12, 2005, over Gilching (near Munich), Germany.

During this flight campaign, the SAR data were collected in X-VV. Preliminary results were presented already in [15] and [16]. This letter includes the extended and final analyses

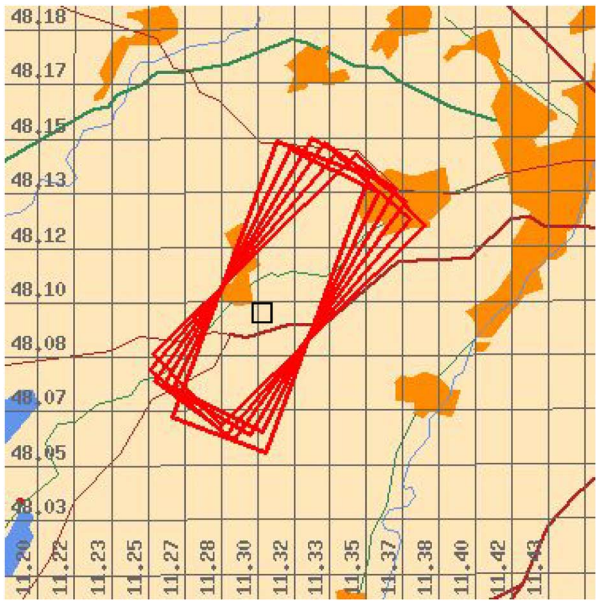

Fig. 3. Footprints of six SAR data takes acquired during the flight campaign on May 12, 2005, over Gilching (near Munich), south Germany. The longer side of each footprint is parallel to the flight direction. The park car is marked as a square.

Fig. 4. One of the test cars that were used in the experiments: VW Golf V, which is the most popular car in Germany.

of experimental data. The footprints of SAR data collections are shown in Fig. 3. In total, six overflights were performed, with one flight for each heading.

This flight campaign aimed at the coverage of the whole range of aspect angles in fine approximately 0.35° angular resolution by carefully selecting the six flight headings or SAR look angles (in 5° steps) and placing seven cars of the same type (Fig. 4)—VW Golf V, which is a popular car in Europe—with different orientations (in 30° steps) (see Fig. 5). For example, the overflight with the SAR look angle of 0° will produce aspect angles of 0°, 30°, 60°, 90°, 120°, 150°, and 180° for a car; the next SAR look angle of 5° will produce aspect angles of 5°, 35°, 65°, 95°, 125°, 155°, and 185° (where 185° is equivalent to 175° due the assumed car symmetry); and so on. Thus, the whole range of aspect angles from 0° to 180° is covered in 5° steps or resolution. Additionally, the look processing for each aspect angle separately, as described in the previous section, allows further to increase the aspect angle resolution from 5° to the fine approximately 0.35° resolution.

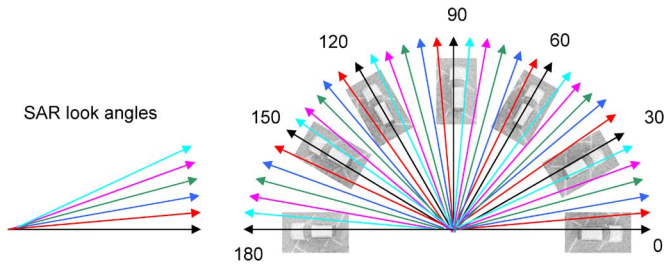

Fig. 5. Experiment setup aimed at the coverage of the whole range of aspect angles in fine approximately 0.35° resolution by carefully selecting the six SAR look angles (in 5° steps) and placing seven cars of the same type—VW Golf V—with different orientations (in 30° steps).

SAR measurements of these seven test cars after focusing, calibration, look processing, and antenna pattern correction for individual looks were used to derive the RCS versus aspect angle plot. The maximum absolute calibration error was ± 2 dB $\cdot$ m^2. These limits of the error were confirmed by the measurements of the corner reflectors (provided by colleagues from DLR Microwave and Radar Institute) that were used during the experiments. The incidence angle was approximately $\theta = 41.5°$ (middle of the swath) and varied in the range of 0.4° (see Table I). The aspect angle for the back, side, and front views is, by definition, 0°, 90°, and 180°, respectively. These angles are further called "favorable" angles. The whole aspect angle range of 180° was covered with only six overflights. It can be assumed that cars are symmetric along the main (driving) axis. The σ_0 was approximately equal to -17 dB for the car park surface (paved road).

The final assembly of all the RCS measurements for X-VV depending on the aspect angle are presented in Fig. 6. We see that the RCS values of the cars in back view (aspect angles ranging from $-10°$ to 25°) are mainly above 0 dB $\cdot$ m^2 (except one outlier) and range from 0 to 16 dB $\cdot$ m^2. For cars in front view (aspect angles ranging from 170° to 190°), RCS values are mainly above 0 dB $\cdot$ m^2 (again except one outlier) and range from -2 to 13 dB $\cdot$ m^2. For cars in side view (aspect angles ranging from 85° to 100°), RCS values are mainly above 0 dB $\cdot$ m^2 (except few outliers) and range from -5 to 19 dB $\cdot$ m^2. The RCS for cars in slanted view (aspect angles ranging from 30° to 80° and from 100° to 170°) have a mean value of below 0 dB $\cdot$ m^2 and range from -18 to 9 dB $\cdot$ m^2. The total mean of RCS for all aspect angles is equal to 0.5 dB $\cdot$ m^2, and the standard deviation is 7.1 dB $\cdot$ m^2. The fundamental behavior of the RCS pattern can be explained as follows. A car in front, side, or back view has a relatively large area, which directly reflects the radar wave and relatively large area of double reflection between the car and the road and, thus, a large resultant RCS value. In slanted views of a car, these reflection areas are much smaller due to the geometry of a car, and thus, the RCS is much lower. This explanation is confirmed, e.g., by visualization of simulation results [10].

Aside from the general dependence on the aspect angle, the RCS (Fig. 6) shows a great variation on small changes of aspect angle, e.g., up to 10 dB $\cdot$ m^2 for 0.35°. We have to note that the fundamental RCS pattern and great variation were also observed during simulations [10]. For the quantification of the measurement error, the experiment design (Fig. 5) has

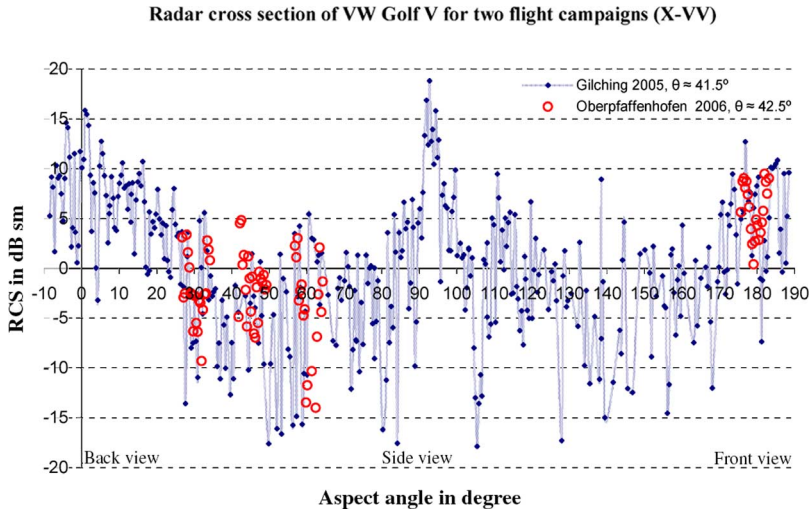

Fig. 6. RCS (in decibel square meters) of VW Golf V depending on the aspect angle for X-VV with an angular resolution of 0.35° for two flight campaigns. The absolute RCS values between the campaigns cannot be compared due to different incidence angles.

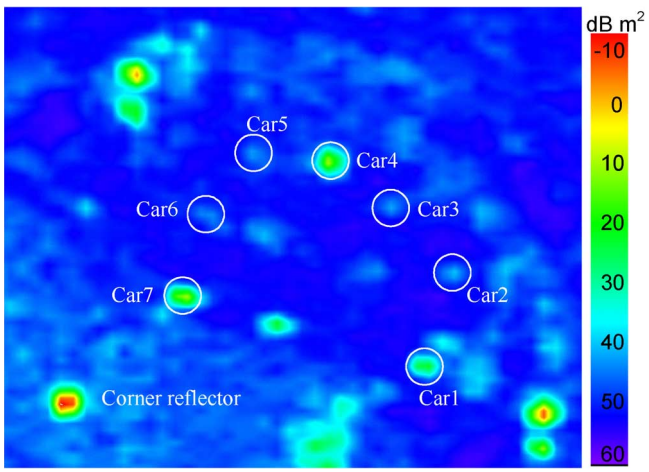

Fig. 7. Incoherent mean of all look images of the car park with seven cars for one overflight of the 2005 campaign. The cars had been placed in different orientations. The multilook image was used to support the search of the peak position of the car, particularly, for weak targets. The colors give an impression of the RCS in decibel square meters.

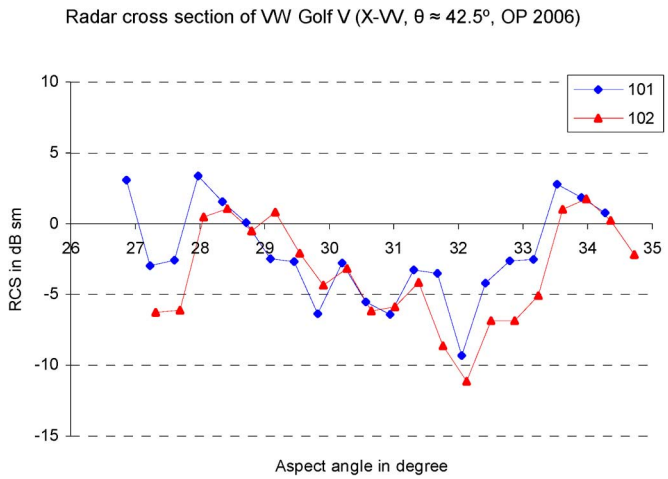

Fig. 8. Radar cross section of VW Golf V for repeat overflights 101 and 102 for flight campaign 2006.

foreseen about 2° overlap between each pair of overflights. Only the boundary looks of the two closest (with the flight direction angle difference of 5°) overflights overlap. These repeated measurements were used to estimate the experimental noise of the first flight campaign. The mean difference of the two measurements for the replicated aspect angle range of $33 \times 2^\circ$ is equal to 0.48 dB $\cdot$ m^2, and the standard deviation is 3.0 dBm^2. The bias of the repeated measurements is under the calibration error of 2 dB $\cdot$ m^2. A little bit higher standard deviation (overestimated value) can result from the usage of only boundary looks, which are known to be much noisier as the middle ones. So, this error analysis shows that the great variability of RCS on small aspect angle changes is mainly due to the aspect angle change.

In order to facilitate the detection of weak targets (e.g., slanted views of cars) in noisy low-resolution look images, a multilook image (incoherent mean of all looks) for each overflight was created (Fig. 7). This auxiliary image was of great help in determining the peak position of weak targets, thus increasing the accuracy and robustness of RCS measurements in separate looks.

B. Second Flight Campaign

To confirm the reproducibility of RCS measurements, particularly, for "unfavorable" aspect angles, where the separation of signal and noise can be difficult, the second flight campaign was conducted on May 8, 2006, over Oberpfaffenhofen (near Munich), south Germany, with two repeated overflights with the same flight track. This time due to limited resources, four test cars again of the same type (Fig. 4) were placed in an empty car park with the following aspect angles: 30°, 45°, 60°, and 180°, which exhibited lower RCS values during the first campaign. In order to improve the signal-to-noise ratio (or to make the detection of weak targets (e.g., cars in slanted view) in SAR image easier and more robust), a car park with much lower σ_0 and a lower flight altitude had been chosen (Table I). Unfortunately, we have not met exactly the same incidence angle for both flight campaigns (41.5° versus 42.5°),

and the absolute RCS of both experiments cannot be compared. However, two repeat overflights with the same heading at this flight campaign allowed us to verify the reproducibility of our RCS measurements. As an example, the RCS values for one of these cars are presented in Fig. 8. We see that the RCS difference of the two overflights is in the range of calibration accuracy (± 2 dB $\cdot$ m^2). The mean difference of the two measurements for all four cars was about 1.1 dB $\cdot$ m^2, and the standard deviation is 2.1 dB $\cdot$ m^2 for the following aspect angle ranges: $30^\circ \pm 3.5^\circ$, $45^\circ \pm 3.5^\circ$, $60^\circ \pm 3.5^\circ$, and $180^\circ \pm 3.5^\circ$. The fine aspect angle resolution was again obtained by look processing. This error analysis confirms once more that the experimental error is in the range of the calibration error, and thus, our both experiments have produced significant results.

VI. Conclusion

The RCS analysis shows that the largest RCS values and, thus, the greatest chance for high probability of detection are for cars in back, front, and side views. Slanted views can exhibit very low RCS values and are therefore less suitable for the car detection. So, the cars only in "favorable" aspect angles can be detected reliably. Furthermore, it was shown that the RCS suffers from the great variation on small changes of aspect angle of up to 10 dB $\cdot$ m^2 for 0.35°.

Of course, all these conclusions are based on the analysis of one type of car and particular incidence angles that were used in the experiments, but our experience with other types of passenger cars and incidence angles confirms these general conclusions [15], [16]. The error analysis for both flight campaigns has showed the significance of the results.

With flight campaigns, the full range of parameters on which the RCS depends and all types of cars cannot be covered. Therefore, a modeling of cars and simulation is required. The data set for the VW Golf V that was provided in this letter can be used to validate the model that was used in the simulation process.

The derived RCS will serve as an input for the development of the car detection algorithms, which will be used in the processing of TerraSAR-X data for traffic monitoring applications.

Acknowledgment

The authors would like to thank H. Breit (from the DLR Remote Sensing Technology Institute), D. Klement, and E. Kemptner (both from the DLR Microwave and Radar Institute) for the theoretical discussions; R. Horn, R. Scheiber, and C. Laux (all from DLR Microwave and Radar Institute) for their efforts in planning the flight campaign, data acquisition, and SAR data processing; D. Klement and E. Kemptner for providing and placing the corner reflectors in the car park; and finally, F. Meyer, D. Weihing, and A. Laika (all from Technical University Munich) for the positioning of the cars.

References

[1] S. Buckreuss, W. Balzer, P. Mühlbauer, R. Werninghaus, and W. Pitz, "The TerraSAR-X satellite project," in *Proc. IGARSS*, Toulouse, France, Jul. 2003, pp. 3096–3098.

[2] J. Mittermayer and H. Runge, "Conceptual studies for exploiting the TerraSAR-X dual receive antenna," in *Proc. IGARSS*, Toulouse, France, Jul. 2003, pp. 2140–2142.

[3] H. Runge and M. Ruhé, "Verkehrsmonitoring mit dem deutschen Fernerkundungssatelliten TerraSAR-X," *DLR Nachr.*, vol. 106, pp. 10–15, 2003.

[4] H. Runge, M. Eineder, G. Palubinskas, S. Suchandt, and F. Meyer, "Traffic monitoring with TerraSAR-X," in *Proc. Int. Radar Symp.*, Berlin, Germany, Sep. 2005, pp. 629–634.

[5] F. Meyer and S. Hinz, "The feasibility of traffic monitoring with TerraSAR-X—Analyses and consequences," in *Proc. IGARSS*, Anchorage, AK, Sep. 2004, pp. 3096–3098.

[6] S. Suchandt, G. Palubinskas, H. Runge, M. Eineder, F. Meyer, and R. Scheiber, "An airborne SAR experiment for ground moving target identification," I/W3in *Proc. ISPRS Hannover Workshop— High Resolution Earth Imag. Geospatial Inf.*, Hannover, Germany, May 2005, vol. XXXVI.

[7] S. Suchandt, G. Palubinskas, R. Scheiber, F. Meyer, H. Runge, P. Reinartz, and R. Horn, "Results from an airborne SAR GMTI experiment supporting TSX traffic processor development," in *Proc. IGARSS*, Seoul, Korea, Jul. 2005, vol. IV, pp. 2949–2952.

[8] G. Palubinskas, F. Meyer, H. Runge, P. Reinartz, R. Scheiber, and R. Bamler, "Estimation of along-track velocity of road vehicles in SAR data," in *Proc. Image and Signal Process. Remote Sens. XI SPIE*, L. Bruzzone, Ed., 2005, vol. 5982, pp. 59 820T-9 59 830T-1.

[9] S. Suchandt, M. Eineder, R. Müller, A. Laika, S. Hinz, F. Meyer, and G. Palubinskas, "Development of a GMTI processing system for the extraction of traffic information from TerraSAR-X data," in *Proc. 6th Eur. Conf. Synthetic Aperture Radar*, Dresden, Germany, May 2006, pp. 1–4.

[10] D. Hounam, S. Baumgartner, K. H. Bethke, M. Gabele, E. Kemptner, D. Klement, G. Krieger, G. Rode, and K. Wägel, "An autonomous, non-cooperative, wide-area traffic monitoring system using space-based radar (TRAMRAD)," in *Proc. IGARSS*, Seoul, Korea, Jul. 2005, pp. 2917–2920.

[11] R. K. Raney, T. Freeman, R. W. Hawkins, and R. Bamler, "A plea for radar brightness," in *Proc. IGARSS*, Pasadena, CA, Aug. 1994, pp. 1090–1092.

[12] *Electronic Warfare and Radar Systems Engineering Handbook*, 1997. NAWCWPNS TP 8347.

[13] R. Bamler and B. Schättler, "SAR Data Acquisition and Image Formation," in *SAR Geocoding: Data and Systems*, G. Schreier, Ed. Karlsruhe, Germany: Wichmann, 1993, pp. 53–101.

[14] R. Scheiber, A. Reigber, A. Ulbricht, K. P. Papathanassiou, R. Horn, S. Buckreuß, and A. Moreira, "Overview of interferometric data acquisition and processing modes of the experimental airborne SAR system of DLR," in *Proc. IGARSS*, Hamburg, Germany, Jun./Jul. 1999, vol. 1, pp. 35–37.

[15] G. Palubinskas, H. Runge, and P. Reinartz, "Radar signatures of road cars," in *Proc. IGARSS*, Anchorage, AK, Sep. 2004, vol. 2, pp. 1498–1501.

[16] G. Palubinskas, H. Runge, and P. Reinartz, "Radar signatures of road vehicles: Airborne SAR experiments," in *Proc. SAR Image Anal., Modeling and Tech. VII SPIE*, F. Posa, Ed., 2005, vol. 5980, pp. 598 006-1-598 006-11.